

Hannu J. Aronen, MD, PhD • Inna E. Gazit, MD • David N. Louis, MD • Bradley R. Buchbinder, MD  
Francisco S. Pardo, MD • Robert M. Weisskoff, PhD • Griffith R. Harsh, MD  
G. Rees Cosgrove, MD • Elkan F. Halpern, PhD • Fred H. Hochberg, MD • Bruce R. Rosen, MD, PhD

## Cerebral Blood Volume Maps of Gliomas: Comparison with Tumor Grade and Histologic Findings<sup>1</sup>

**PURPOSE:** To assess the utility of magnetic resonance (MR) cerebral blood volume (CBV) maps in the evaluation of gliomas.

**MATERIALS AND METHODS:** CBV maps from 19 patients with histologically proved gliomas were calculated from dynamic MR image sets acquired with echo-planar spin-echo imaging after intravenous injection of gadolinium-based contrast material.

**RESULTS:** The maximum CBV varied from 0.82 to 5.40 in the high-grade group ( $n = 13$ ) and from 1.01 to 1.21 in the low-grade group ( $n = 6$ ). The difference was statistically significant. Maximum CBV was associated with mitotic activity and vascularity, but not with cellular atypia, endothelial proliferation, necrosis, or cellularity.

**CONCLUSION:** MR CBV maps provided diagnostic information not available with conventional MR imaging in six cases and offers a functional parameter for assessing glioma grade and regions of focal activity.

**Index terms:** Brain neoplasms, 13.363 • Magnetic resonance (MR), echo planar, 13.121416 • Magnetic resonance (MR), vascular studies, 13.12144 • Magnetic resonance (MR), volume measurement, 13.12144

*Radiology* 1994; 191:41-51

<sup>1</sup> From the Departments of Radiology (H.J.A., I.E.G., B.R.B., R.M.W., E.F.H., B.R.R.), Pathology (Neuropathology) (D.N.L.), Radiotherapy (F.S.P.), Neurosurgery (G.R.H., G.R.C.), and Neurology (F.H.H.), MGH NMR Center, Massachusetts General Hospital, Charlestown, MA 02129. Received July 21, 1993; revision requested September 9; revision received December 10; accepted December 20. Supported in part by National Institutes of Health grants RO1-CA40303, RO1-HL39810, and PO1-CA48729 and by an industrial grant from Sterling-Winthrop Pharmaceutical Research Division. H.J.A. supported in part by the Academy of Finland; the Cultural Foundation of Finland; the Paulo Foundation, Helsinki, Finland; and National Institutes of Health Fogarty International Center grant F05 TW04520. Address reprint requests to H.J.A.  
© RSNA, 1994

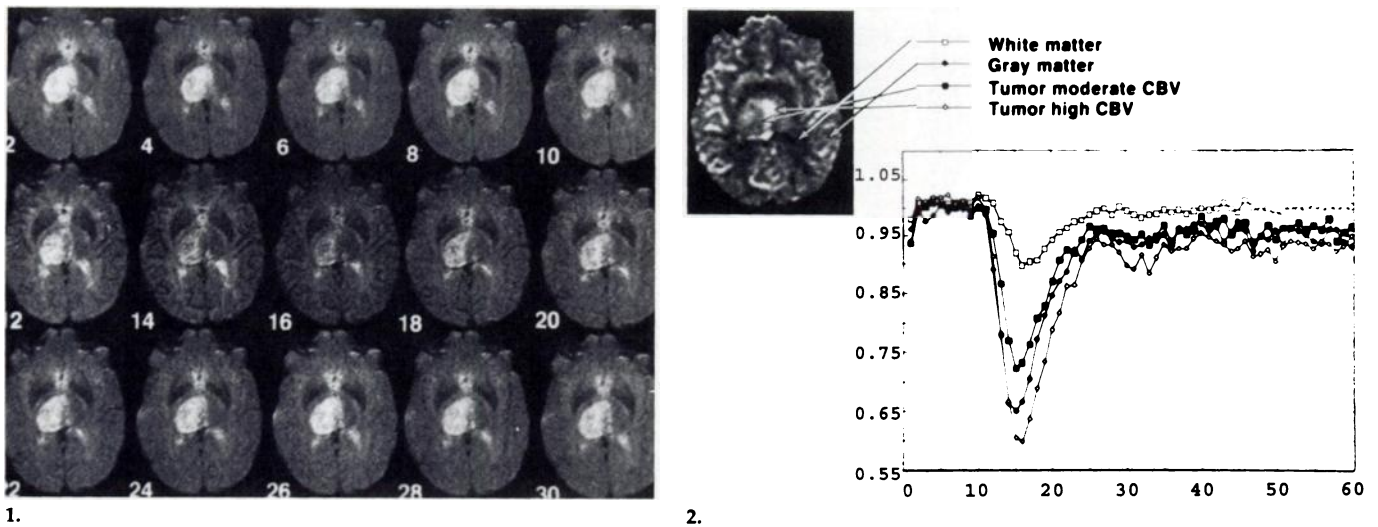
**G**LIOMAS are the most common primary neoplasms of the central nervous system (1). Despite improvements in radiation therapy and chemotherapy, the overall prognosis for patients with glioma has remained poor, especially in those with high-grade tumors (2). Because therapeutic approaches for these tumors differ considerably according to tumor grade, the development of techniques capable of accurately depicting tumor grade in vivo is important for the determination of appropriate treatment strategies. Gliomas are typically heterogeneous, and histologic samples obtained at biopsy may be subject to sampling error (1,3). An unfortunate choice of biopsy site or one too small may result in an incorrect assignment of a low tumor grade and thus mislead determinations of optimum treatment strategies.

The development of computed tomographic (CT) and magnetic resonance (MR) imaging technology and intravenous contrast material techniques has led to improved accuracy in the detection and characterization of various brain tumors. The use of gadolinium-based contrast material has substantially increased the specificity and sensitivity of brain MR imaging (4-7), and, at present, gadolinium-based contrast agents are routinely used in MR imaging of the brain when tumors are suspected. However, important limitations exist with conventional imaging techniques in the diagnosis of primary brain tumors. Measurements of T1, T2, and proton density, or their combinations, are not sufficiently specific to help distinguish between low- and high-grade tumors (8). Moreover, contrast enhancement or the lack thereof is not specific for gliomas and does not provide a clear-cut differential diagnosis between high- and low-grade gliomas. Nevertheless, in general terms, greater likelihood for contrast enhancement exists in high-grade tumors (9,10).

Another problem with conventional techniques results from the heterogeneity often found in gliomas. Even after contrast material administration, conventional MR or CT images may not show the most malignant tumor area and may mislead MR imaging- or CT-directed biopsies. The use of fluorodeoxyglucose as a tracer in functional positron emission tomography (PET) studies, however, may substantially improve the assessment of the prognosis (11,12), grading of gliomas (13), and selection of biopsy sites in brain tumors (14).

Studies of human neoplasms have demonstrated that increased malignancy is associated with increased vascularity (15-17). Gliomas, especially when high grade, are highly vascular. An assessment of the microvascular structures of these tumors, including the proliferation of the endothelial cells that line tumor capillaries, is a component of most histologic grading systems. The assessment of vascular proliferation as a primary grading criterion has been employed with encouraging results (18). Contrast material-enhanced angiographic techniques have been used for many years to demonstrate some of the features related to tumor neovascularization, particularly with respect to pathologic vessel formation. However, these methods cannot be the basis of a quantitative classification system for the microvasculature because of their insufficient spatial resolution at a real capillary level. Moreover, contrast-enhanced angiography cannot provide the tomographic images that are useful in obtaining relative quantitative evaluations of the extent and quantity of pathologic vessel formation.

**Abbreviations:** CBV = cerebral blood volume, PET = positron emission tomography, ROI = region of interest, WHO = World Health Organization.



**Figures 1, 2.** (1) Series of echo-planar spin-echo images of a patient with a right thalamic tumor. The images were acquired immediately before, during, and after the first pass of a bolus of gadopentetate dimeglumine through the brain. Images were obtained at a rate of one per second; every second image is shown. When the contrast material reaches the brain, it causes signal loss (middle row). Regions of greater CBV exhibit greater signal loss, as demonstrated by the greater regional blood volume of gray matter compared to white matter. The tumor has heterogeneous signal loss, greatest in its medial aspect due to focal elevated CBV. Numbers indicate sequence in image acquisition. (2) CBV map (left) calculated on a pixel-by-pixel basis from the data set partially presented in 1. Higher CBV is represented by higher signal intensity (white area) on the CBV map. Note the relatively high CBV in the normal cortical gray matter and the deep gray nuclei, as well as within the medial portion of the tumor. Graph (right) shows normalized signal intensity curves during the transit of the contrast material through the brain for normal gray and white matter regions and for two areas within the tumor. Numbers on x axis are seconds. Numbers on y axis are normalized signal intensity.

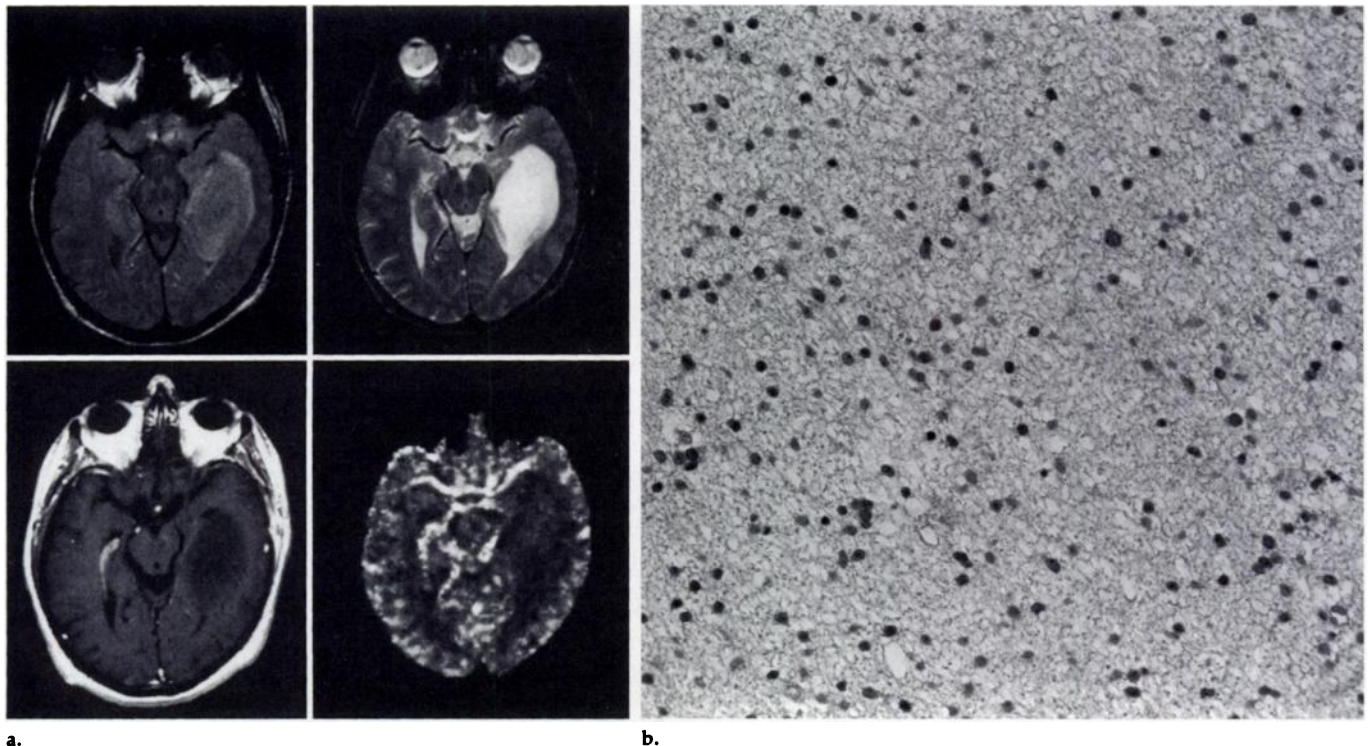


**Figure 3. Patient 5.** (a) Proton-density-weighted (2,000/30) (top left), T2-weighted (2,000/80) (top right), and contrast-enhanced T1-weighted (700/20) (bottom left) MR images; the CBV map of a left temporal lobe tumor is shown in the bottom right. The appearance of the tumor on all studies was consistent with that of a low-grade glioma, which was verified at biopsy. The tumor is nonenhancing and shows a relatively low blood volume on the CBV map. Note the relatively high CBV content in the normal choroid plexus and larger vessels. (b) Histologic specimen. A grade 2 astrocytoma was diagnosed. The tumor was mildly hypercellular (cellularity = 1) with rare, thin-walled capillaries (vascularity = 1).

Recent developments in echo-planar imaging technology (19) and functional MR imaging techniques (20) have made it possible to obtain measurements of the microvascula-

ture within brain lesions (21). Cerebral blood volume (CBV) maps calculated from MR images are particularly sensitive for depicting the microvasculature (22,23) and can enable the

detection of neovascularization at the capillary level, as well as its quantification in relative terms (21,24).

The purpose of the present study was to assess the value of CBV maps

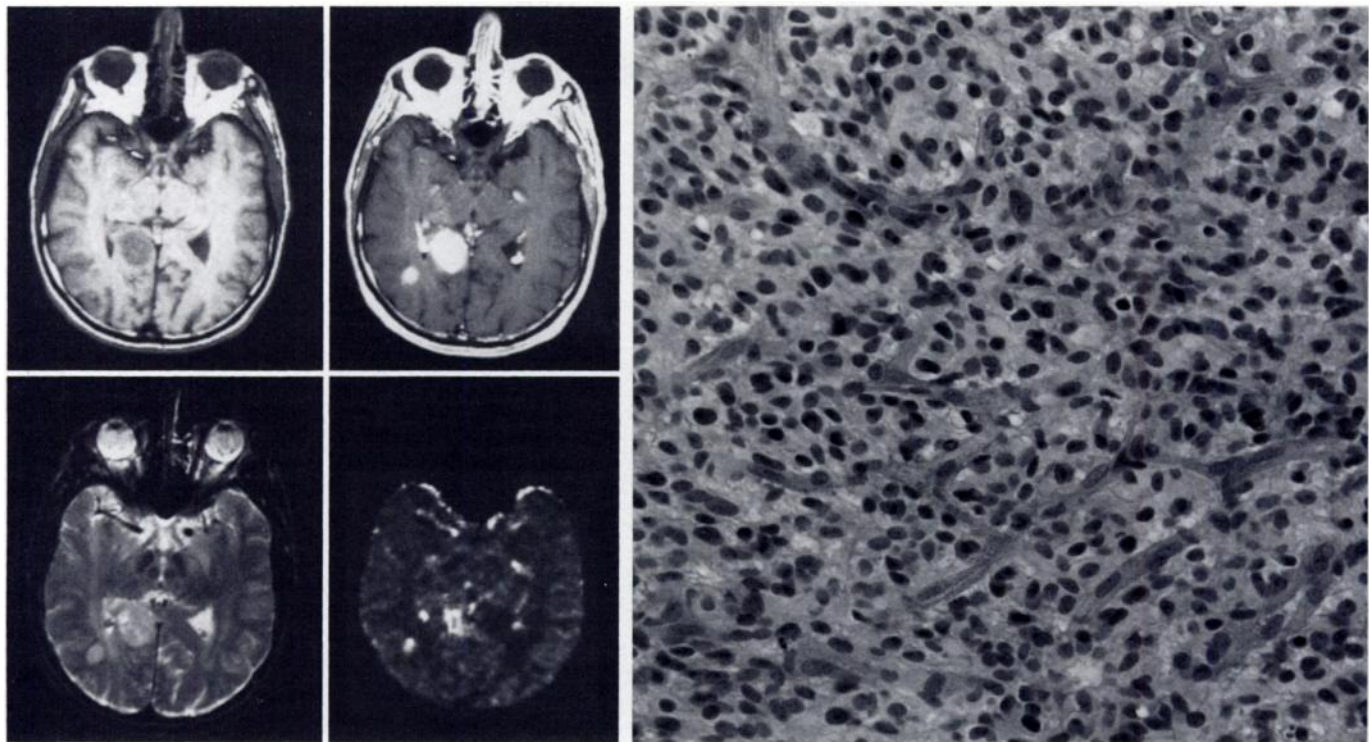
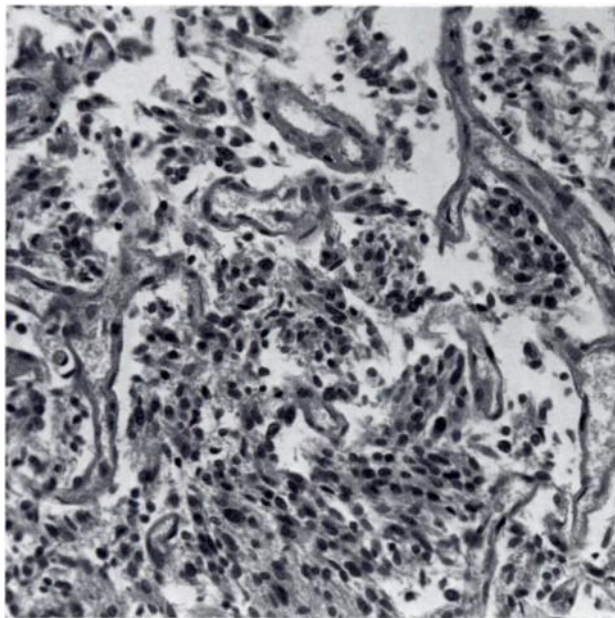


**Figure 4. Patient 19.** (a) Pre- and postcontrast T1-weighted MR images (700/20) (top left and right, respectively), T2-weighted MR image (2,000/80) (bottom left), and CBV map (bottom right) of two enhancing foci in the right temporal lobe. The CBV map, obtained after injection of 0.2 mmol/kg of gadodiamide, shows elevated CBV in both foci, suggesting a high-grade glioma. The diagnosis was confirmed at surgery. (b, c) Corresponding histologic specimens show increased capillary density in the high-grade oligoastrocytoma. (b) Densely cellular areas (cellularity = 3) with numerous branching vessels (vascularity = 3) and (c) many wider vessels and conspicuous endothelial cells (vascularity = 3) are seen. Thus, the tumor demonstrated both heterogeneity of vessel diameter and high vascularity at histopathologic examination and heterogeneously increased CBV.



**(b, c)** Corresponding histologic specimens show increased capillary density in the high-grade oligoastrocytoma. (b) Densely cellular areas (cellularity = 3) with numerous branching vessels (vascularity = 3) and (c) many wider vessels and conspicuous endothelial cells (vascularity = 3) are seen. Thus, the tumor demonstrated both heterogeneity of vessel diameter and high vascularity at histopathologic examination and heterogeneously increased CBV.

calculated from MR images for diagnosing and grading gliomas and to compare the results with those from conventional MR imaging and histologic examination. We also evaluated whether any subcomponents of pathologic assessment were correlated with the functional MR imaging measurements. In particular, we wanted to determine whether CBV maps could provide information not obvious on conventional MR images of gliomas, assess the ability of the functional technique to evaluate

ranges of microvascular CBV values within these lesions, and evaluate whether this range or the highest identified CBV value (maximum tumor CBV) could aid in the evaluation of glioma grade.

**MATERIALS AND METHODS**

Nineteen patients were studied. Patients ranged in age from 23 to 69 years; there were 13 men and six women. Approval for the study was obtained from the Subcommittee on Human Research at

Massachusetts General Hospital, and informed consent was obtained for all subjects. Patients with histologically verified gliomas who had not undergone any major therapeutic interventional procedures were included in the study.

Conventional MR images and CBV maps were acquired during the same procedure to allow for an exact comparison of the results obtained. All MR images were obtained at 1.5 T with a Signa imager (GE Medical Systems, Milwaukee, Wis) retrofitted with Instascan EP technology (Advanced NMR, Wilmington, Mass) (25). Before imaging was performed, an 18-gauge catheter was inserted into a large peripheral vein, usually the antecubital vein. A saline drip was used to maintain the vein's patency.

Sagittal T1-weighted localizing images were acquired first. Then, unenhanced axial T1- and T2-weighted images were obtained for each patient. Single-section studies were acquired for eight patients, whereas images from eight sections were collected in the remaining 11. Axial sections were selected from the unenhanced images for dynamic MR imaging. Gadopentetate dimeglumine (Magnevist; Ber-

lex, Wayne, NJ) (0.1 or 0.2 mmol/kg in 16 patients), gadodiamide (Omniscan; Nycomed, distributed by Sanofi-Winthrop, New York, NY) (0.1 and 0.2 mmol/kg in two patients), or gadoteridol (Prohance; Squibb Diagnostics, Princeton, NJ) (0.1 and 0.2 mmol/kg in one patient) was power-injected (Medrad, Pittsburgh, Pa) at a rate of 5 mL/sec through the angiocatheter. The two patients who received gadodiamide were participating in a phase III trial study of the safety and efficacy of a higher cumulative dose (0.3 mmol/kg) of the contrast agent. Three patients received two consecutive injections of contrast material during imaging to saturate the interstitial space in tumors with a suspected disrupted blood-brain barrier (26). In these cases, the CBV map was calculated from images acquired after the second injection.

For the single-section studies ( $n = 8$ ), a series of images (60 images in 60 seconds) was obtained at 1,000-msec intervals by using a lipid-suppressed spin-echo echo-planar pulse sequence (repetition time = 1,000 msec, echo time = 100 msec [1,000/100], 64-msec image acquisition window) before, during, and after injection of each contrast agent (20). Lipid suppression was used to suppress subcutaneous fat, which can be superimposed on the brain due to the large chemical shift artifact seen with echo-planar imaging. Eleven patients were studied using multisection data acquisition. In these patients, eight sections were collected by using 1,500/100 (32 images for each section in 48 seconds). A section thickness of 7 mm was used for all studies (full width at half maximum, sinc-shaped radio-frequency section excitation for square section profile). We used a  $256 \times 128$  matrix and a  $20 \times 40$ -cm field of view, resulting in an in-plane voxel size of  $1.5 \times 1.5$  mm. After data collection, CBV maps were derived on a voxel-by-voxel basis from the dynamic image sets.

Several raw data images from a single section are shown in Figure 1. The starting and ending points of the first pass transit of the contrast agent through the brain were identified by using the time-activity curve of the means of signal magnitude of pixels covering the whole-brain tissue on the section as a region of interest (ROI). Before the starting point of the first-pass circulation (seen as a drop in signal), a representative number of baseline points were selected and their average calculated for each voxel as a baseline measure for signal intensity ( $S_0$ ). On a voxel-by-voxel basis, signal intensity ( $S$ ) was converted to changes in T2 relaxation rate,  $-\ln(S/S_0)/$  echo time. Previous experiments and theoretical data have demonstrated that  $\Delta R_2$  is approximately linearly proportional to the concentration of contrast material in tissue (23,27,28). Relative CBV maps were generated by numerical integration of relative concentration ( $\Delta R_2$ ) for the first-pass bolus through each voxel based on kinetic principles for nondiffusible tracers (29,30). A  $3 \times 3$  voxel smoothing kernel was applied to all raw images before integration. Image processing was performed with a Sun SPARCstation; approximately 2–5 minutes

**Table 1**  
Comparison of CBV Values and Normal Gray Matter/White Matter Ratio

Patient No./ Age (y)/ Sex	Pathologic Diagnosis	Range of CBV Values	Gray Matter/ White Matter Ratio
1/38/F	Oligoastrocytoma (2)	1.10–1.21	2.28
2/28/F	Oligoastrocytoma (2)	1.05–1.13	2.47
3/25/M	Astrocytoma (2)	0.96–1.17	2.75
4/38/M	Astrocytoma (2)	0.96–1.01	1.58
5/36/M	Astrocytoma (2)	0.78–1.02	1.86
6/37/M	Astrocytoma (2)	0.50–1.14	2.24
7/26/F	Astrocytoma (3)	2.07–3.83	2.23
8/66/M	Astrocytoma (4)	0.34–3.46	2.73
9/60/F	Astrocytoma (4)	0.20–1.77	2.31
10/48/F	Astrocytoma (3)	0.21–2.11	2.63
11/62/M	Astrocytoma (3)	0.91–5.31	2.32
12/64/F	Astrocytoma (4)	0.18–5.40	2.75
13/48/M	Oligoastrocytoma (3)	1.43–4.84	2.44
14/45/F	Astrocytoma (4)	0.70–0.82	2.27
15/62/M	Astrocytoma (3)	0.18–1.55	1.85
16/69/M	Astrocytoma (4)	0.12–3.73	2.36
17/63/M	Oligoastrocytoma (3)	0.77–5.31	2.60
18/50/M	Astrocytoma (3)	0.51–4.73	2.35
19/50/M	Oligoastrocytoma (4)	1.49–4.48	1.96

Note.—Numbers in parentheses are tumor grade.

were required to smooth and integrate the functional time course data. In Figure 2, the calculated CBV map is shown along with the actual signal intensity curves in various areas inside both tumor and normal brain.

Because the susceptibility contrast CBV mapping method yields a relative rather than absolute value of CBV, comparison among patients is facilitated by reference to an internal standard. In analogy to a previous PET study (31), normal white matter in the contralateral hemisphere was used as this reference. To calculate the ratios between cortical gray and white matter, ROIs were defined on proton-density-weighted images, when possible, and then applied to the CBV maps. To calculate the relative CBV ratios of tumor/white matter, the ROIs were defined on conventional MR images by a radiologist (H.J.A.). These ROIs were applied to the CBV maps, and the ratios were calculated by dividing the mean CBV of the tumor by that of the normal contralateral white matter. When previously unseen areas of increased CBV were detected on the CBV maps, new ROIs were defined and tumor/white matter ratios calculated by reference to the white matter regions as described above. Various areas of CBV were analyzed within each lesion and the areas of the highest and lowest CBV identified.

All conventional MR images were analyzed by two radiologists (H.J.A., B.R.B.), who used previously published criteria to classify gliomas (32–34). The presence or absence of the following features was noted: enhancement, delineation of the lesion, cyst formation, necrosis, hemorrhage, and calcifications. In addition, edema and lesions were evaluated for overall homogeneity or heterogeneity. After analyzing the conventional MR images and CBV maps, the information gained from each set was compared. Tu-

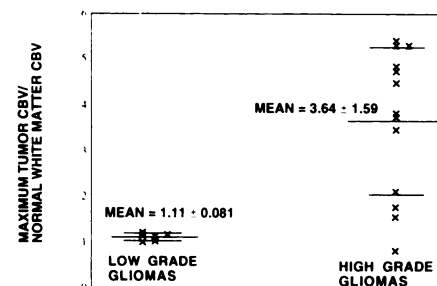


**Figure 5.** Maximal tumor/normal white matter CBV ratio. The ratio is higher in the high-grade gliomas than in the low-grade gliomas. The highest CBV value (mean  $\pm$  standard deviation) in the low- ( $n = 6$ ,  $1.11 \pm 0.081$ ) and high- ( $n = 13$ ,  $3.64 \pm 1.59$ ) grade glioma groups were compared to that of the normal white matter. The difference in means is statistically significant ( $P = .0001$ , Student  $t$  test for unequal variances). Mean and 1 standard deviation lines are shown for each group.

mor extent was carefully analyzed on both MR images and CBV maps, and discordances, if any, were registered. A consensus concerning additional information provided with the CBV maps, but not obvious on the conventional MR images, was then determined.

At least one sample was obtained from each tumor at biopsy or surgical resection. All tumor specimens were examined by a neuropathologist (D.N.L.) and graded according to the World Health Organization (WHO) (35) and Dumas-Duport (36) grading systems. Astrocytomas were diffuse and fibrillary and were classified as grades 2–4. Oligodendrogliomas were classified as either low grade or anaplastic and as grades 2–4 according to the WHO system. Mixed gliomas (“oligoastrocytomas”) were classified according to the

**Table 2**  
**Summary of Histologic Findings**

Patient No.	Diagnosis	Histologic Finding					
		Atypia	Mitosis	Endothelial Proliferation	Necrosis	Vascularity Score	Cellularity Score
1	Oligoastrocytoma (2)	Yes	Yes	No	No	1	2
2	Oligoastrocytoma (2)	Yes	No	No	No	1	3
3	Astrocytoma (2)	Yes	No	No	No	1	1
4	Astrocytoma (2)	Yes	No	No	No	1	2
5	Astrocytoma (2)	Yes	No	No	No	1	1
6	Astrocytoma (2)	Yes	No	No	No	1	1
7	Astrocytoma (3)	Yes	Yes	No	No	2	2
8	Astrocytoma (4)	Yes	Yes	No	Yes	3	3
9	Astrocytoma (4)	Yes	Yes	No	Yes	2	3
10	Astrocytoma (3)	Yes	Yes	No	Yes	1	2
11	Astrocytoma (3)	Yes	Yes	No	No	1	2
12	Astrocytoma (4)	Yes	Yes	Yes	Yes	3	3
13	Oligoastrocytoma (3)	Yes	Yes	No	No	3	2
14	Astrocytoma (4)	Yes	Yes	Yes	Yes	2	3
15	Astrocytoma (3)	Yes	Yes	No	No	1	2
16	Astrocytoma (4)	Yes	Yes	No	Yes	1	2
17	Oligoastrocytoma (3)	Yes	Yes	Yes	Yes	3	3
18	Astrocytoma (3)	Yes	Yes	No	No	1	2
19	Oligoastrocytoma (4)	Yes	Yes	Yes	Yes	3	3

**Table 3**  
**Findings at Conventional MR Imaging**

Patient No.	Enhancement	Necrosis	Edema	Cyst Formation	Tumor Delineation*	Heterogeneity	Hemorrhage	Mass Effect
1	No	No	No	No	III	No	No	No
2	No	No	No	No	Well	No	No	No
3	No	No	No	No	III	No	No	No
4	No	No	No	No	Well	No	No	Local
5	No	No	No	No	Well	Yes	No	No
6	No	No	No	No	III	Yes	No	Local
7	Yes	No	No	No	Well	No	Yes	Local
8	Yes	Yes	Yes	No	Well	Yes	Yes	Local
9	Yes	Yes	Yes	No	III	Yes	No	Local
10	Yes	Yes	Yes	No	Well	Yes	No	Local
11	No	No	No	No	III	Yes	No	Local
12	Yes	Yes	Yes	No	III	Yes	No	Local
13	Yes	Yes	Yes	No	III	Yes	Yes	No
14	Yes	No	Yes	No	III	No	No	Local
15	Yes	No	Yes	No	III	Yes	No	Local
16	Yes	Yes	Yes	Yes	III	Yes	No	Local
17	Yes	No	Yes	No	III	Yes	Yes	Local
18	No	No	No	Yes	Well	Yes	No	Local
19	Yes	No	No	No	III	Yes	No	Local

\* III = ill defined, well = well defined.

grade of both components. Grade 2 tumors were designated as low-grade gliomas, and grade 3 and 4 tumors were designated as high-grade gliomas.

The following histopathologic parameters were assessed for each tumor: the presence or absence of cytologic atypia, mitoses, endothelial proliferation, and necrosis. Endothelial proliferation was diagnosed when at least two endothelial cells comprised the width of the capillary wall. The presence of any so-called "glomeruloid vessels" was also noted. In addition, vascularity was assessed on a scale of 1 to 3, with 1 = vascularity of that of the normal brain (Fig 3b), 2 = moderately increased vascularity, and 3 = greatly increased vascularity characteristic of some glial tumors (Fig 4b, 4c). Necrosis was fur-

ther characterized as "pseudopalisading around necrosis" when tumor cells were aggregated around relatively small zones of necrosis or as "bland necrosis" when large areas of tumor necrosis were present with thromboses and without adjacent, proliferating tumor. An estimate of cellularity was also made, with 1 = minimally increased cellularity (Fig 3b), 2 = intermediate cellularity, and 3 = densely cellular tumor (Fig 4b, 4c).

The Student *t* test was used to analyze the relationship of the glioma grade to each of the maximum tumor CBV values, the range of CBV values, and the gray matter/white matter ratio, and the relationship of glioma type to maximum tumor CBV. Simple linear regression was used to analyze the relationship of indi-

vidual pathologic measures (atypia, mitotic activity, endothelial proliferation, necrosis) to maximum tumor CBV. An analysis of variance was used to analyze the relationship of vascularity and cellularity to the maximum tumor CBV. A stepwise, multiple linear regression was used to analyze the relationship of all the pathologic measures (atypia, mitotic activity, endothelial proliferation, necrosis, vascularity, and cellularity) to the maximum tumor CBV. The Student *t* test was used to analyze the relationship of the individual conventional MR imaging measurements to the maximum tumor CBV. A stepwise multiple linear regression was used to analyze the relationship of all conventional MR imaging measurements to the maximum tumor CBV. The Fisher exact test was used to analyze the relationship of the individual MR imaging measurements to the tumor grade.

To compensate for the multiple comparison issue, the conservative Bonferroni correction was applied to the six analyses of the relationship of the individual pathologic measures to the maximum tumor CBV. Findings were considered significant if  $P < .008$ . Similarly, the Bonferroni correction was applied to the eight analyses of the relationship of individual conventional MR imaging measurements to tumor grade. Findings were considered significant if  $P < .006$ .

The stepwise regression analyses were performed to determine which, if any, of the significant individual relationships of maximum tumor CBV to the individual measures were independent of the other measures and which seemed to be redundant. As such, these analyses were exploratory in nature, and no adjustment for multiple comparisons was made.

## RESULTS

There were no side effects related to either rapid contrast material injection or the contrast agents used in the study. The pathologic diagnoses are listed in Table 1. In all cases, the WHO and Dumas-Duport grades were identical. Table 1 documents pathologic diagnoses and the maximum and minimum CBV values within each glioma. There is considerable variability in the range of CBV values both within and between these tumors. In normal brain regions, the mean of the gray matter/white matter ratio was  $2.32 \pm 0.32$ ; this ratio did not differ between high-grade ( $2.37 \pm 0.27$ ) and low-grade ( $2.20 \pm 0.42$ ) gliomas ( $P = .29$ ).

### Relationship of Maximum Tumor CBV and Tumor Grade

The maximum tumor CBV in the high-grade tumor group ( $n = 13$ ) varied from 0.82 to 5.40 (mean,

3.64 ± 1.59). The maximum tumor CBV value in the low-grade tumor group (*n* = 6) varied from 1.01 to 1.21 (mean, 1.11 ± 0.081). This difference was statistically significant (*P* = .0001, Student *t* test for unequal variances) (Fig 5). A typical low-grade astrocytoma is shown in Figure 3. The tumor exhibits low CBV. A high-grade glioma is shown in Figure 4; heterogeneous high- and medium-CBV areas are seen in the tumor. In high-grade gliomas, 12 of the 13 tumors had maximum tumor CBV greater than 1.5. In low-grade gliomas, no tumor had a maximum CBV greater than 1.5.

### Relationship of CBV Range and Tumor Grade

The CBV range in the high-grade tumor group was 0.12–5.22, with a mean of 2.94 ± 1.50. In the low-grade tumor group, however, the CBV range was narrower, 0.05–0.64, with a mean of 0.22 ± 0.22. This difference was statistically significant (*P* = .0001, Student *t* test for unequal variances) (Table 1).

### Relationship of CBV, Vascularity, and Cellularity

When analyzing the relationship of vascularity to maximum tumor CBV, we found the overall difference in the mean of the maximum tumor CBV to be statistically significant (*P* = .009). The five tumors categorized as showing high vascularity had a mean maximum CBV of 4.70 ± 0.76. The three with medium vascularity had a mean maximum CBV of 2.14 ± 1.54, while the 11 with low vascularity had a mean maximum CBV of 2.19 ± 1.61. Pairwise comparisons in maximum tumor CBV measurements indicated that tumors of greatly increased vascularity (category 3) differed significantly from tumors of lesser vascularity (categories 1 and 2) (*P* = .027). Tumor cellularity was not statistically significantly related to the maximum tumor CBV (*P* = .10).

### Comparison of CBV Maps and Histologic Findings

The histologic features of the tumors are listed in Table 2. When analyzing the individual relationships of maximum tumor CBV and each of the four subcomponents of the Daumas-Duport classification system (cellular atypia, mitotic activity, endothelial proliferation, and necrosis), the maximum CBV was associated with mitotic

**Table 4**  
**Tumor Location and Appearance on Conventional MR Images and CBV Maps**

Patient No.	Location of Tumor*	Findings at MR Imaging	Findings at CBV Mapping
1	L frontotemporal	Homogeneous, non-enhancing	Homogeneous low CBV
2	R frontal	Homogeneous, non-enhancing	Homogeneous low CBV
3	L frontal	Homogeneous, non-enhancing	Homogeneous low CBV
4	L occipital	Homogeneous, non-enhancing	Homogeneous low CBV
5	L temporal	Heterogeneous, non-enhancing	Heterogeneous low CBV
6	L temporal	Heterogeneous, non-enhancing	Heterogeneous low CBV
7	R thalamic	Homogeneous, minimally enhancing	Heterogeneous high CBV
8	L parietal	Enhancing rim, necrotic center, surrounding edema	High CBV in rim, low CBV in necrotic center and edema zone
9	R temporal	Enhancing rim, necrotic center	High CBV rim, low CBV in necrotic center
10	R frontoparietal	Enhancing rim, necrotic center, surrounding edema	High CBV rim, low CBV in necrotic center and edema zone
11	L temporal	Heterogeneous, non-enhancing	Focal area of high CBV in an otherwise low-CBV tumor
12	R frontal	Heterogeneous enhancement, mass effect, surrounding edema	Heterogeneous high CBV in rim, high CBV in nodular satellite lesion, low CBV in necrotic center and edema zone
13	L frontal	Mildly heterogeneous, partly enhancing	Focal regions of high CBV in areas of hyperintensity seen at T2-weighted imaging, with and without associated enhancement
14	L parietooccipital	Homogeneous enhancement, surrounding edema	Homogeneous low tumor CBV, low CBV in edema zone
15	L temporooccipital	Heterogeneous enhancement, surrounding edema	Heterogeneous low and moderately high CBV
16	L parietooccipital	Heterogeneous enhancement, surrounding edema	Heterogeneous high and low CBV in tumor, low CBV in edema zone
17	R frontal	Heterogeneous enhancement, surrounding edema	High CBV (mainly in non-enhancing regions) low CBV in edema zone
18	L frontal, parietal, temporal	Heterogeneous, small cystic component, nonenhancing	Focal high-CBV region in otherwise low-CBV tumor
19	R temporal	Two apparently discrete tumor foci, mildly heterogeneous enhancement	Heterogeneous high and intermediate CBV in both lesions

\* Note.—L = left, R = right.

activity (*P* = .006). When analyzing the overall relationship of maximum tumor CBV and all six parameters evaluated from the pathologic samples (cellular atypia, mitotic activity, endothelial proliferation, necrosis, vascularity, and cellularity), mitotic activity and vascularity are significantly (*P* = .025 and .013, respectively) associated with maximum tumor CBV. Of the 19 gliomas, 14 pure astrocytomas were found. Oligodendroglial components were found in five tumors. No statistically significant difference existed in maximum tumor CBV between these two subgroups

(2.65 ± 1.70 for pure astrocytomas and 3.39 ± 2.05 for oligoastrocytomas) (*P* = .44).

### Relationship of Findings at Conventional MR Imaging and Tumor Grade

Table 3 describes the findings at MR imaging; the Fisher exact test was used to analyze the relationship of the individual findings to tumor grade. Tumor grade was not associated with enhancement (*P* = .001). The relationships between tumor grade and edema (*P* = .011) and tu-

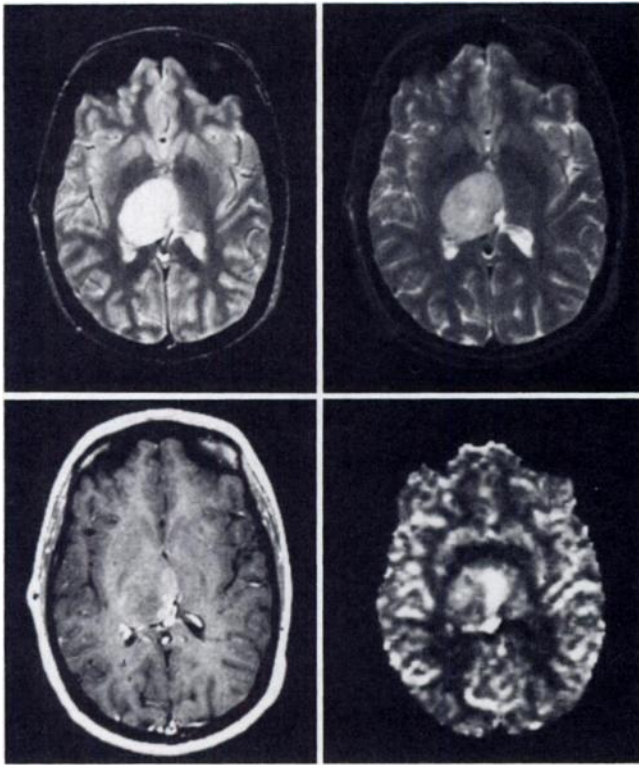


**Figure 6. Patient 7.** MR images and CBV map obtained from the same patient as in Figures 1 and 2. On the proton-density-weighted (2,000/30) (top left) and T2-weighted (2,000/80) (top right) images, the tumor is rather homogeneous. The tumor enhances only slightly after administration of contrast material (bottom left). The CBV map (bottom right) shows varying areas of elevated CBV within the tumor, consistent with a high-grade glioma. The diagnosis of a grade 3 astrocytoma was verified at biopsy.

mor heterogeneity ( $P = .046$ ) were not considered to be statistically significant, as they did not reach the Bonferroni criterion. Tumor grade was not associated with necrosis ( $P = .11$ ), cyst formation ( $P = 1.000$ ), delineation ( $P = .62$ ), hemorrhage ( $P = .26$ ), or mass effect ( $P = .079$ ).

#### Comparison of CBV Maps and Conventional MR Images

Stepwise multiple linear regression was used to analyze the relationship of maximum tumor CBV to the MR imaging findings listed earlier. The only variable associated with maximum tumor CBV was tumor heterogeneity ( $P = .023$ ). When we compared maximum tumor CBV values for enhancing ( $n = 11$ ) and nonenhancing ( $n = 8$ ) tumors, the mean value was found to be higher in the first group ( $3.39 \pm 1.60$ ) than in the second ( $2.09 \pm 1.82$ ). However, this difference did not reach statistical significance ( $P = .12$ ).

Findings from conventional MR images and CBV maps are presented in Table 4. Features depicted on the CBV maps that were not obvious on

MR images were found for six of the 19 patients (patients 7, 11–13, 17, and 18). In these patients, an area of high CBV was identified in nonenhancing or enhancing tumor regions, or both. In patients 11 and 18, the CBV maps indicated the presence of a focal high-CBV area within a tumor otherwise characterized by low CBV. In both cases, a high-grade tumor was confirmed at histologic examination.

In patient 7, a right thalamic tumor was homogeneous on conventional MR images and only minimally enhancing on contrast-enhanced T1-weighted images. On the CBV map, however, this glioma showed marked high CBV and heterogeneity, indicating the high-grade nature of the tumor (Fig 6). This was confirmed at biopsy.

In patient 13, T2-weighted images demonstrated a region of hyperintensity, which could have represented edema, tumor, or both. The CBV map revealed high CBV in this region, suggestive of active tumor rather than edema alone (Fig 7).

In patient 17, who had a large tumor of the right frontal lobe that had been diagnosed 8 years previously,

MR images revealed some tumor enhancement after administration of contrast material. The CBV map, however, revealed areas of high CBV that did not enhance on the conventional MR images, indicative of a probable malignant dedifferentiation of the tumor. In this patient, CBV mapping results were concordant with those obtained from a PET flow study that used  $C^{15}O_2$  as a tracer. The high-grade nature of the areas of high CBV within the lesion was confirmed after a subsequent debulking operation by means of histologic analysis of a number of surgical samples from the tumor (Fig 8).

In patient 12, CBV mapping yielded information about a multifocal, right frontal lobe tumor that was not obvious from the conventional MR studies. While the MR images revealed several enhancing areas within the tumor, the CBV maps indicated the heterogeneity of the measured CBV that existed within these regions. A debulking operation was subsequently performed. Tissue samples from the two foci with highest CBV values showed rich vascularity at histologic analysis, and the presence of a grade 4 astrocytoma was confirmed (Fig 9). Several samples from the tumor were obtained in a later debulking operation. The results of the histologic analysis were consistent with the findings at CBV mapping, which showed areas of high capillary density and a high tumor grade.

#### DISCUSSION

We were able to demonstrate an association between the areas of high CBV identified with functional MR imaging techniques and the pathologic grade of gliomas. We were also able to demonstrate an association between the identification of high-CBV areas within a tumor on CBV maps and the grade of tumor vascularity as determined with pathologic specimens. The formation of functioning capillaries, however, is composed of many steps: Tumor angiogenesis is a complex process presumed to involve the close interaction of tumor cells, capillary endothelial cells, and the extracellular matrix. Endothelial proliferation alone may or may not lead to tube formation of functioning capillaries. Because CBV maps are sensitive for only the perfused part of capillary formation, they measure only functioning capillaries. It is therefore not surprising that a statistically significant correlation could not be demonstrated between the identifica-

tion of high-CBV areas and the finding of endothelial thickening (endothelial proliferation) of vessel walls at histologic examination. However, an association between the maximum tumor CBV and the histologically determined degree of vascularity was demonstrated.

When stepwise multiple linear regression was used to investigate the dependence of high CBV on the sub-components listed in the Daumas-Duport pathologic grading system, the functional MR imaging findings proved to be associated only with mitotic activity, not with necrosis or endothelial proliferation. Thus, information provided by CBV mapping may be somewhat independent from that provided by the pathologic classification systems routinely used in the diagnosis of gliomas. Interestingly, the maximum tumor CBV did not significantly differ between pure astrocytomas and oligoastrocytomas, indicating that CBV mapping may not be used to differentiate between these tumor types, a matter of importance since different therapeutic options exist for these patient groups (2,37).

In this study, an association was found between vascularity and maximum tumor CBV. The mean maximum CBV value for tumors determined to contain regions of high vascularity differed significantly from that for tumors of medium or low vascularity. However, the maximum CBV values did not differ between the low and medium vascularity groups. In the five patients with highly vascular tumors, the maximum CBV values were high, ranging from 3.46 to 5.40 (mean, 4.70). Both tumor heterogeneity and the techniques by which brain tissue samples are acquired from human patients should be considered when interpreting these results.

For homogeneous low-grade gliomas, our results suggest that the actual sampling site is not crucial. In all six low-grade gliomas with low vascularity, the maximum CBV values were 1.01–1.21, showing excellent correlation. Heterogeneous tumors, however, are great sources of potential sampling error, because the area of greatest tumor activity may not be sampled. This is the likely explanation for the fact that, in this study, some of the tumors were histologically determined to be of low or medium vascularity, while CBV mapping revealed areas of high CBV. This also may explain why no differences were found between the mean maximum CBV values for low and medium vascularity groups.

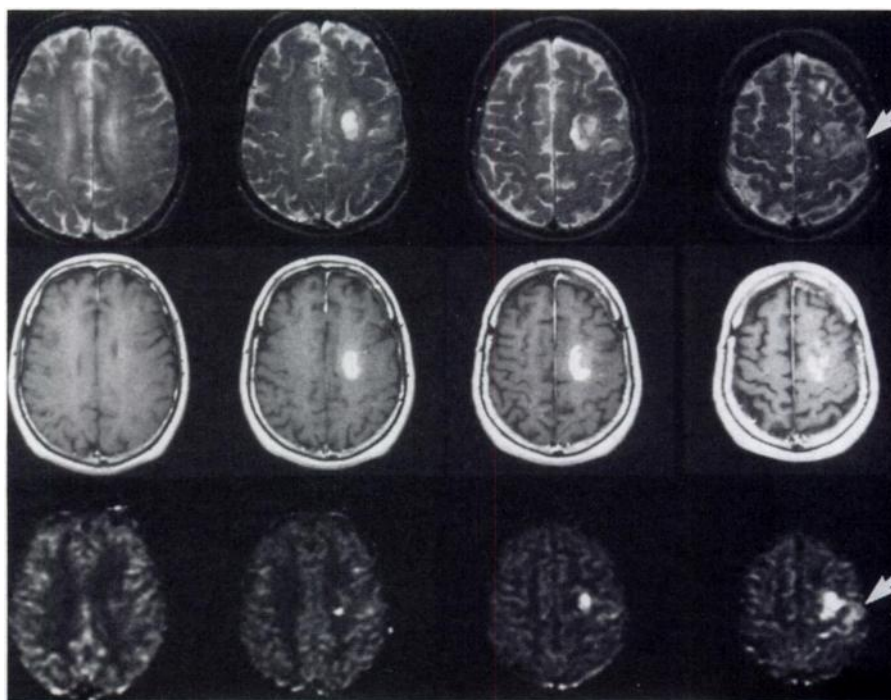


**Figure 7. Patient 13.** T2-weighted MR images (2,000/80) (top row), contrast-enhanced T1-weighted images (700/20) (middle row), and multisecton CBV maps (bottom row) from a patient with a grade 3 oligoastrocytoma. Four of the eight sections obtained are shown. The areas of high CBV identified on the CBV maps show substantial overlap with areas of increased signal intensity on the T2-weighted images but are partially distinct from enhancing regions on the T1-weighted images. The diagnosis was confirmed at biopsy. Focal regions of high CBV are present in regions of high signal intensity on T2-weighted images (arrows), with and without associated edema; this could indicate tumor, edema, or both. High CBV suggests the presence of active tumor.

Although endothelial proliferation has been used as a diagnostic criterion for most pathologic grading systems (1,35,36,38), only a few imaging studies (39) have attempted to use cerebral hemodynamics to grade gliomas. Because neovascularization is a characteristic of gliomas, an imaging method capable of characterizing the microvasculature throughout the tumor could offer physiological information that is coupled to tumor activity. The appearance of gliomas on a CBV map is complex (Table 4), and variations in CBV within a given tumor or tumor region are common, especially in high-grade lesions. The ability of CBV maps to depict tumor heterogeneity and indicate the region with the highest CBV offers a useful parameter, maximum tumor CBV, with which to characterize gliomas.

The mean CBV value of a tumor depends on the proportion of high- and low-CBV areas within it, probably partially reflecting the proportion of various tissue components (such as active tumor area and necrosis) within the lesion. Thus, the mean tumor CBV may not provide the best indication of areas of highest CBV in heterogeneous tumors, such as high-

grade gliomas. Because high-CBV areas may represent active tumor, if not the areas of greatest malignancy, we have chosen to use several tumor CBV measurements to identify regions of maximum tumor CBV, as well as minimum CBV values, rather than to determine one mean CBV value for the entire lesion. All six low-grade tumors were nonenhancing and had low CBV and a narrow range of CBVs. However, nonenhancing tumors containing areas of high CBV were eventually proved to be of high grade (patients 11 and 18). In patient 14, a CBV map of an enhancing tumor with low CBV, but medium vascularity, most likely reflects, at least partially, an underestimation of the tumor's actual CBV value. The identification of any area of high CBV provided a specific marker for the existence of a high-grade glioma. In the high-grade group, the relative CBV content and its range was usually greater than those in the low-grade group, indicating varied regions of capillary density within these lesions.

In this study, the maximum tumor CBV obtained with CBV maps was associated with findings at conventional MR imaging only in the vari-

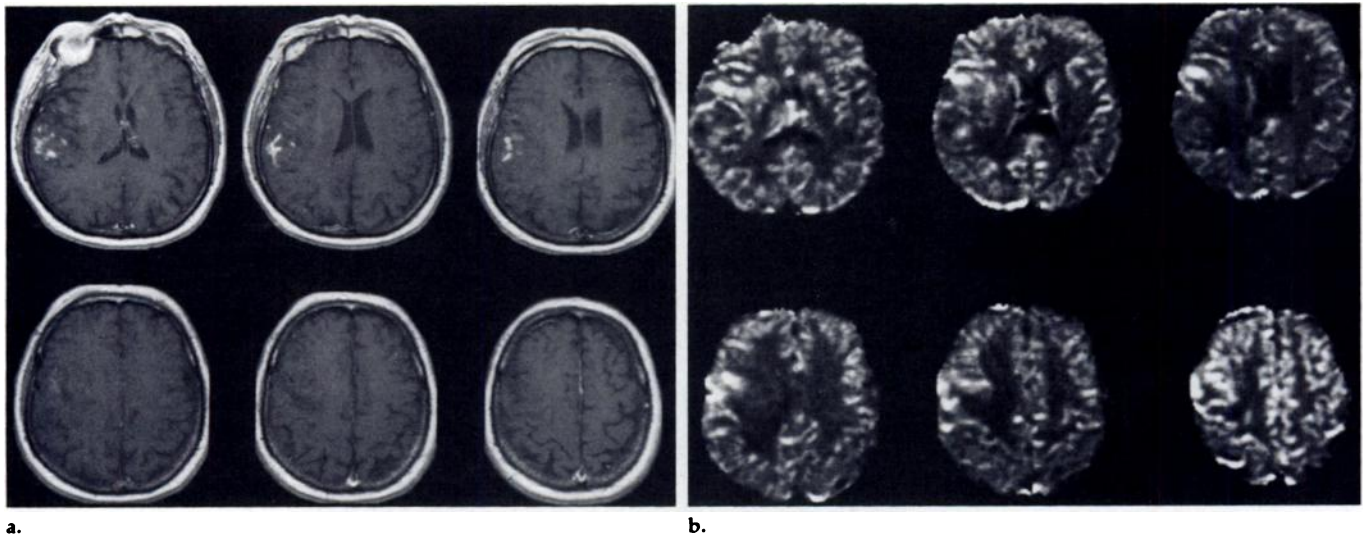


**Figure 8. Patient 17.** (a) Contrast-enhanced T1-weighted MR images (700/20) and (b) CBV maps acquired from eight sections through a right frontal lobe tumor. Six of the eight sections are shown. MR images show multinodular enhancement in a poorly demarcated tumor. CBV maps show high-CBV areas that are partially distinct from enhancing tumor areas (for example, the images in the bottom row display high CBV regions in the absence of contrast enhancement). After the tumor was debulked, a high-grade astrocytoma was verified at histologic examination.

able that described tumor heterogeneity. In a previous investigation with conventional MR imaging and CT techniques, a correlation was found to exist between enhancing regions, malignant neovascularity, and endothelial proliferation (40). Vascularity was not assessed. In our study, tumors that enhanced on the MR images generally had the highest CBV. However, this difference was not statistically significant. These findings emphasize that such pathophysiologic properties as disruption of the blood-brain barrier (for which contrast-enhanced studies are sensitive) and capillary density (measured with CBV mapping) may be present in the same tumor or tumor region.

Although we found an association between tumor enhancement at conventional MR imaging and glioma grade, the results proved that the measurement of tumor CBV does not reproduce tumor enhancement characteristics. Enhancement alone cannot serve to quantify neovascularization, but only to localize some of its related features. As discussed earlier, the spin-echo techniques employed in CBV mapping are particularly sensitive for demonstrating the microvasculature (22), although the echo-planar technique we used maintains some sensitivity to very large vessels such as the middle cerebral artery (Fig 3) (41). When the blood-brain barrier is intact, CBV mapping techniques provide a correct measure of tumor microvasculature in relative terms. When the blood-brain barrier is disrupted, as is the case in many high-

grade gliomas, CBV mapping performed with use of small gadolinium chelates may underestimate the real microvascular blood volume. This results from the methods used in producing blood volume maps, which assume a compartmentalization between the vascular and extravascular spaces (42).

In enhancing tumors, the decreased concentration gradient of the contrast material between intra- and extravascular compartments decreases the susceptibility effect during the first pass of the contrast material. At the same time, because of the accumulation of the gadolinium-based contrast material within the extracellular space during the first pass of the agent, T1 is shortened, leading to an increase in the measured signal intensity. Both of these factors decrease the measured signal loss that is otherwise created by the susceptibility effect of the compartmentalized contrast material. Tumor blood flow and the relative volume of extracellular space may also play a part in this underestimation. Currently, we are investigating techniques to minimize or eliminate this underestimation in enhancing tumors (26).

Despite these theoretical concerns, high-CBV areas were identified in both enhancing and nonenhancing tumor regions. In the enhancing areas, CBV content was found to vary substantially, even within the same tumor. The identification of high-CBV areas within these enhancing tumors was not surprising, since substantial susceptibility contrast has been ob-

served in other tissues lacking a tight compartmentalization between capillary and extravascular spaces (eg, the myocardium). In myocardium, for instance, the first-pass extraction fraction of gadolinium and dysprosium chelates is substantially greater than that seen in primary intraaxial lesions characterized by a defective blood-brain barrier (43).

The ratio obtained in this study between cortical gray and white matter, approximately 2.3, correlated well with that obtained in previous PET studies (44), as well as with findings in a recent study that utilized MR imaging CBV mapping techniques based on rapid gradient-echo imaging with a conventional imager (45). Recent reports from the PET literature have indicated the use of both cortical gray and white matter regions as normal reference areas for analyzing the energy metabolism of gliomas (11,31). In this investigation, we found that identifying a corresponding white matter area on the proton-density-weighted image provided the basis for a suitable method of semiquantitation of CBV maps. It also has been suggested that normal cortical gray matter may be used as a reference area when interpreting perfusion MR imaging susceptibility studies (46). However, because normal cortical gray matter is only 2–5 mm thick, the partial volume effect and contamination from the surrounding structures may interfere with this technique. In this series, all CBV maps were evaluated together with corresponding conventional MR images, and the ar-

areas of high CBV within the tumors were identified.

Some normal structures, such as the choroid plexus and great vessels, show a high CBV in CBV mapping studies. It is important that these normal structures are not interpreted as false-positive findings. In addition, all CBV maps were analyzed by means of semiquantitative measurement of regional tumor CBV areas and comparison (division) of these values with that of normal contralateral white matter. Good correspondence was noted between both methods of evaluation.

### CONCLUSION

Because of tumor location, stereotaxic biopsies or bulk resections of malignant brain tumors cannot always be performed. Biopsy sites based solely on conventional imaging methods may, in some instances, provide critically limited information about the nature of heterogeneous gliomas. A noninvasive imaging method for characterizing the functional properties of malignant processes stands to be of great benefit to clinical practice. CBV mapping can help grade gliomas and depict varying areas of hemodynamic activity within tumors and surrounding tissue. Thus, this technique may provide a valuable adjunct to the clinical management of primary gliomas. ■

### References

- Russell D, Rubenstein L. Tumours of central neuroepithelial origin. In: Rubenstein LJ, ed. Pathology of tumours of the nervous system. Baltimore, Md: Williams & Wilkins, 1989; 83-350.
- Black PM. Brain tumors. *N Engl J Med* 1991; 324:1471-1476, 1555-1564.
- Glantz MJ, Burger PC, Herndon JE II, et al. Influence of the type of surgery on the histologic diagnosis in patients with anaplastic gliomas. *Neurology* 1991; 41:1741-1744.
- Carr DH, Brown J, Bydder GM, et al. Intravenous chelated gadolinium as a contrast agent in NMR imaging of cerebral tumors. *Lancet* 1984; 1:484-486.
- Felix R, Schörner W, Laniado M, et al. Brain tumors: MR imaging with gadolinium-DTPA. *Radiology* 1985; 156:681-688.
- Schwaighofer BW, Klein MV, Wesbey G, Hesselink JR. Clinical experience with routine Gd-DTPA administration for MR imaging of the brain. *J Comput Assist Tomogr* 1990; 14:11-17.
- Healy ME, Hesselink JR, Press GA, Middleton MS. Increased detection of intracranial metastases with intravenous Gd-DTPA. *Radiology* 1987; 165:619-624.
- Just M, Thelen M. Tissue characterization with T1, T2, and proton density values: results in 160 patients with brain tumors. *Radiology* 1988; 169:779-785.
- Brant-Zawadzki M, Berry I, Osaki L, Brasch R, Murovic J, Norman D. Gd-DTPA in clinical MR of the brain. I. Intraaxial lesions. *AJNR* 1986; 8:781-788.
- Brant-Zawadzki M. Pitfalls of contrast-enhanced imaging in the nervous system. *Magn Reson Med* 1991; 22:243-248.
- Alavi JB, Alavi A, Chawluk J, et al. Positron emission tomography in patients with glioma: a predictor of prognosis. *Cancer* 1988; 62:1074-1078.
- Di Chiro G. Positron emission tomography [<sup>18</sup>F]fluorodeoxyglucose in brain tumors: a powerful diagnostic and prognostic tool. *Invest Radiol* 1986; 22:360-371.
- Di Chiro G, DeLaPaz RL, Brooks RA, et al. Glucose utilization of cerebral gliomas and positron emission tomography. *Neurology* 1982; 32:1323-1329.
- Hanson MW, Glantz MJ, Hoffman JM, et al. FDG-PET in the selection of brain lesions for biopsy. *J Comput Assist Tomogr* 1991; 15:796-801.
- Brem S, Cotran R, Folkman J. Tumor angiogenesis: a quantitative method for histologic grading. *J Natl Cancer Inst* 1972; 48:347-356.
- Weidner N, Semple JP, Welch WR, Folkman J. Tumor angiogenesis and metastasis: correlation in invasive breast carcinoma. *N Engl J Med* 1991; 324:1-8.
- Macchiarini P, Fontanini G, Hardin MJ et al. Relation of neovascularisation to metastasis of non-small-cell lung cancer. *Lancet* 1992; 340:145-146.
- Brem S. The role of vascular proliferation in the growth of brain tumors. *Clin Neurosurg* 1976; 23:440-453.
- Mansfield P. Multi-planar image formation using NMR spin echos. *J Phys* 1977; C10:L55-L58.
- Belliveau JW, Kennedy DN, McKinstry RC, et al. Functional mapping of the human

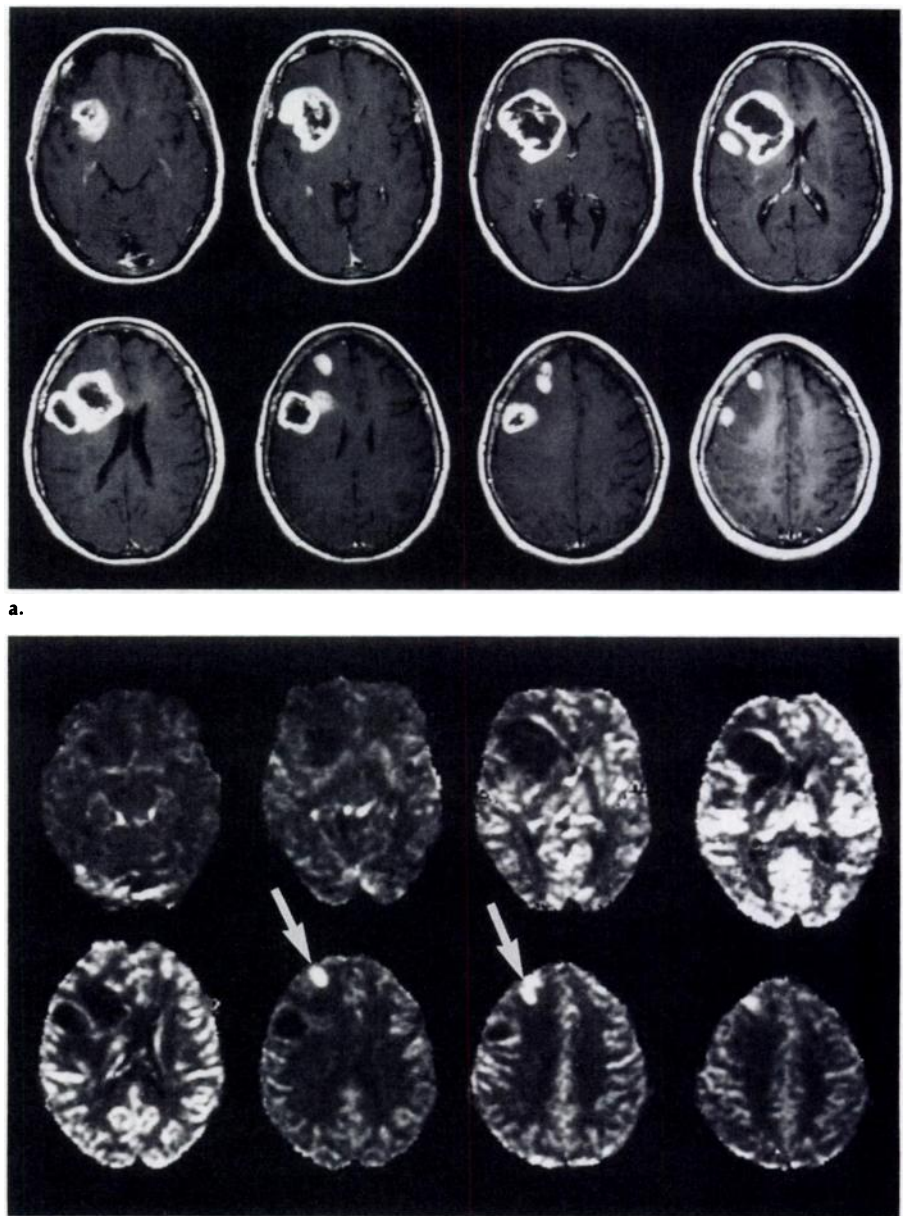


**Figure 9. Patient 12.** (a) Contrast-enhanced T1-weighted MR images (700/20) and (b) multi-section CBV maps obtained before surgical resection of a high-grade astrocytoma with multifocal enhancement. Regions of varying CBV were noted within the enhancing area. Biopsy material obtained from the region of the highest CBV (arrows in b) exhibited high capillary density and a high tumor grade.

- visual cortex using magnetic resonance imaging. *Science* 1991; 254:716-719.
21. Rosen BR, Belliveau JW, Aronen HJ, et al. Susceptibility contrast imaging of cerebral blood volume: human experience. *Magn Reson Med* 1991; 22:293-299.
  22. Fisel CR, Moore JR, Garrido L, Ackerman JL, Rosen BR, Brady TJ. A general model for susceptibility-based MR contrast (abstr). In: *Book of abstracts: Society of Magnetic Resonance in Medicine 1989*. Berkeley, Calif: Society of Magnetic Resonance in Medicine, 1989; 324.
  23. Weisskoff R, Belliveau J, Kwong K, Rosen B. Functional MR imaging of capillary hemodynamics. In: Potchen E, ed. *Magnetic resonance angiography: concepts and applications*. St Louis, MO: Mosby, 1992; 473-484.
  24. Belliveau JW, Rosen BR, Kantor HL, et al. Functional cerebral imaging by susceptibility-contrast NMR. *Magn Reson Med* 1990; 14:538-546.
  25. Rzedzian RR, Pykett IC. Instant images of the human heart using a new whole-body MR imaging system. *AJR* 1987; 149:245-250.
  26. Aronen HJ, Boxerman JL, Goldberg IE, et al. CBV mapping: optimization of contrast dose and imaging sequences (abstr). In: *Book of abstracts: Society of Magnetic Resonance in Medicine 1992*. Berkeley, Calif: Society of Magnetic Resonance in Medicine, 1992; 1129.
  27. Villringer A, Rosen BR, Belliveau JW, et al. Dynamic imaging with lanthanide chelates in normal brain: contrast due to magnetic susceptibility effects. *Magn Reson Med* 1988; 6:164-174.
  28. Majumdar S, Gore JC. Studies of diffusion in random fields produced by variations in susceptibility. *J Magn Reson* 1988; 78:41-55.
  29. Axel L. Cerebral blood flow determination by rapid-sequence computed tomography: a theoretical analysis. *Radiology* 1980; 137:679-686.
  30. Rosen BR, Belliveau JW, Chien D. Perfusion imaging by nuclear magnetic resonance. *Magn Reson Q* 1989; 5:263-281.
  31. Di Chiro G, Brooks R, Bairamian D, et al. Diagnostic and prognostic value of positron emission tomography using [<sup>18</sup>F] fluorodeoxyglucose in brain tumors. In: Reivich M, Alavi A, eds. *Positron emission tomography*. New York, NY: Alan R. Liss, 1985; 291-309.
  32. Dean B, Drayer B, Bird C, et al. Gliomas: classification with MR imaging. *Radiology* 1990; 174:411-415.
  33. Atlas SW. Intra-axial brain tumors. In: Atlas SW, ed. *Magnetic resonance imaging of the brain and spine*. New York, NY: Raven, 1991; 223-326.
  34. Buchbinder BR, Davis KR. MR and CT evaluation of intra-axial brain tumors. In: Thrall JW, ed. *Current practice in radiology*. Philadelphia, Pa: Decker, 1993; 435-461.
  35. Kleihues P, Burger PC, Scheithauer BW. Histological typing of tumours of the central nervous system. 2nd ed. Berlin, Germany: Springer-Verlag, 1993.
  36. Daumas-Duport C, Scheithauer B, O'Fallon J, Kelly P. Grading of astrocytomas: a simple and reproducible method. *Cancer* 1988; 62:2152-2165.
  37. Glass J, Hochberg FH, Gruber ML, Louis DN, Smith D. The treatment of oligodendrogliomas and mixed oligodendroglioma-astrocytomas with PCV chemotherapy. *J Neurosurg* 1992; 76:741-745.
  38. Kernohan J, Mabon R, Svien H. A simplified classification of gliomas. *Proc Staff Meet Mayo Clin* 1949; 25:71-75.
  39. Lammertsma AA, Wise RJS, Jones T. In vivo measurements of regional cerebral blood flow and blood volume in patients with brain tumours using positron emission tomography. *Acta Neurochir (Wien)* 1983; 69:5-13.
  40. Earnest FI, Kelly PJ, Scheithauer BW, et al. Cerebral astrocytomas: histopathologic correlation of MR and CT contrast enhancement with stereotactic biopsy. *Radiology* 1988; 166:823-827.
  41. Hamberg LM, Macfarlane R, Tasdemiroglu E, et al. Measurement of cerebrovascular changes in cats after transient ischemia using dynamic magnetic resonance imaging. *Stroke* 1993; 24:444-451.
  42. Villringer A, Rosen BR, Belliveau JW, et al. Dynamic imaging with lanthanide chelates in normal brain: contrast due to magnetic susceptibility effects. *Magn Reson Med* 1988; 6:164-174.
  43. Wendland MF, Saeed M, Higgins CB. Strategies for differential enhancement of myocardial ischemia using echoplanar imaging. *Invest Radiol* 1991; 26(suppl):236-238.
  44. Lammertsma AA, Wise RJS, Cox TCS, Thomas DGT, Jones T. Measurement of blood flow, oxygen utilisation, oxygen extraction ratio, and fractional blood volume in human brain tumours and surrounding oedematous tissue. *Br J Radiol* 1985; 58:725-734.
  45. Gückel F, Brix G, Deimling M, et al. Assessment of cerebral blood flow dynamics with contrast-enhanced T2\*-weighted gradient-echo images (abstr). In: *Book of abstracts: Society of Magnetic Resonance in Medicine 1992*. Berkeley, Calif: Society of Magnetic Resonance in Medicine, 1992; 1133.
  46. Le Bihan D, Douek M, Argyropoulou M, Turner R, Patronas N, Fulham M. Diffusion and perfusion magnetic resonance imaging in brain tumors. *Top Magn Reson Imaging* 1993; 5:25-31.